Coherent Spatial Variations in the Productivity of Earthquake Sequences in California and Nevada

Daniel T. Trugman[1] and **Yehuda Ben-Zion**[2]

[1]Nevada Seismological Laboratory, Nevada Geosciences, University of Nevada, Reno. Reno NV, USA

[2]Department of Earth Science and Statewide California Earthquake Center, University of Southern California. Los Angeles CA, USA

Corresponding author: Daniel Trugman (dtrugman@unr.edu)

Declaration of Competing Interests

The authors have no known conflicts of interest related to this work.

Abstract

Earthquakes are clustered in space and time, with individual sequences comprised of events linked by stress transfer and triggering mechanisms. At a global scale, variations in the productivity of earthquake sequences – a normalized measure of the number of triggered events – have been observed and associated with regional variations in tectonic setting. Here we focus on resolving systematic variations in the productivity of crustal earthquake sequences in California and Nevada, the two most seismically active states in the western US. We apply a well-tested nearest-neighbor algorithm to automatically extract earthquake sequence statistics from a unified 40-year compilation of regional earthquake catalogs that is complete to ~M2.5. We then compare earthquake sequence productivity to geophysical parameters that may influence earthquake processes, including heat flow, temperature at seismogenic depth, complexity of quaternary faulting, geodetic strain rates, depth to crystalline basement, and faulting style. We observe coherent spatial variations in sequence productivity, with higher values in the Walker Lane of eastern California and Nevada than along the San Andreas Fault system in western California. The results illuminate significant correlations between productivity and heat flow, temperature, and faulting that contribute to the understanding and ability to forecast crustal earthquake sequences in the area.

Introduction

One of the most universal observations of earthquakes is their statistical tendency to cluster in space and time, organizing into sequences of events connected via stress transfer mechanisms (e.g., Ben-Zion, 2008). Earthquake sequences occur in many styles, from classical mainshock-aftershock sequences where a prominent large earthquake triggers a burst of seismic activity that decays in space and time (e.g., Omori, 1894), to swarm-like sequences with extended duration and no dominant mainshock (e.g., Hill, 1977). This intrinsic variability in earthquake clustering reflects the heterogeneous environments where earthquakes occur combined with the inherently complex nature of earthquake sequence dynamics, and it has important implications for hazard.

What causes some earthquake sequences to be highly productive including thousands of triggered events, while other sequences to have low event rates and rapid cessations of seismicity? This question has been long studied using a variety of techniques and datasets, but few definitive answers have been formalized. Singh and Suárez (1988) identified substantial variations in aftershock activity between circum-Pacific subduction zones, while Davis and Frohlich (1991) noted the relative paucity of aftershocks in oceanic ridge-transform systems. Zaliapin *et al.* (2008) developed a nearest-neighbor algorithm to automatically extract earthquake sequences from catalog data, a method that has since been applied to study clustering statistics in southern California (Zaliapin and Ben-Zion, 2013a, 2013b), in areas of induced seismicity (Goebel *et al.*, 2019), and globally (Zaliapin and Ben-Zion, 2016).

Dascher-Cousineau *et al.* (2020) systematically analyzed aftershock event counts derived from a global dataset of large earthquakes. Examining correlations of the results with source- and location-specific parameters, they developed a conceptual model in which aftershock productivity is driven primarily by the availability of nearby faults to activate within the brittle crust, rather than due to source or rupture characteristics, or properties such as temperature and fluid content of the deforming medium. Similarly, Hardebeck (2022) demonstrated that the spatial patterns of aftershocks from select large earthquakes in southern California varies systematically with features derived from stress-change tensors, faulting, and crustal geophysical parameters.

The purpose of this article is to develop improved quantification and understanding of crustal earthquake sequences across California and Nevada, where large variations in productivity are widely appreciated (e.g., Hardebeck *et al.*, 2018), yet both states fall within a single tectonic region for global-scale aftershock forecasting models (Page *et al.*, 2016). This work extends earlier studies centered primarily in southern California by including also northern California and Nevada and by explicit consideration of faulting and crustal property metrics for comparison with sequence productivity. We adopt a more inclusive definition of earthquake sequence productivity (described in detail below) that encompasses all events within a sequence, instead of just direct aftershocks of a prominent mainshock. This allows us to assess earthquake swarms, which are common in California and Nevada, alongside the traditional mainshock-aftershock sequences. The results provide new insights into the characteristics of crustal earthquake sequences in the western US.

Data and Methods

We analyze seismicity catalogs compiled by regional seismic networks in California and Nevada, where there are three authoritative monitoring regions: Southern California, Northern California, and Nevada. We combine earthquake catalogs available from each regional data center (see Data and Resources), removing duplicate events in overlapping regions by prioritizing the origin information of the authoritative agency for the region in which each earthquake occurs. The resulting catalog spans more than 40 years (January 1980 through September 2023) and is complete to ~ **M**2.5 over its duration (Figure S1), with improvements to completeness in more recent years. For this reason, we focus our analysis primarily on **M** ≥ 2.5 earthquakes recorded during this time period. It is important to recognize that the magnitude scales adopted by each regional network are different, which may cause some inconsistencies for smaller earthquakes. We therefore also repeat and confirm the general findings of the analysis described below with only subset of earthquakes with **M** ≥ 3, where network magnitude estimates are broadly consistent with each other and with available moment magnitude estimates (Figure S2).

We isolate earthquake sequences from the unified California-Nevada catalog using the nearest neighbor algorithm defined by Zaliapin et al. (2008) and developed further in subsequent studies (Zaliapin and Ben-Zion, 2013a, 2013b, 2016). In this method, each earthquake *j* is initially associated with a parent earthquake *I* that is its nearest neighbor in space and time, with a distance metric of the form:

$$\boldsymbol{\eta_{ij} = 10^{-bM_i}\, T_{ij}\, R_{ij}^{d}} \ , \tag{1}$$

where $\boldsymbol{M_i}$ is the magnitude of the parent event, and $\boldsymbol{T_{ij}}$ and $\boldsymbol{R_{ij}}$ are the temporal offset and epicentral distances between parent and daughter events. We set the *b*-value to 1.0 and fractal dimension *d* to 1.6, which are representative values for seismicity in this region (Zaliapin and Ben-Zion, 2013b, see also Figure S2). Linked events are partitioned into clusters by imposing a threshold distance $\boldsymbol{\eta_0}$ beyond which neighboring events are separated as in a random process and are referred to as background earthquakes. The choice of this threshold is somewhat subjective; we use a catalog shuffling approach that preserves the magnitude distribution of the input catalog to determine an appropriate value (Goebel *et al.*, 2019, Figure S3). While the precise value of $\boldsymbol{\eta_0}$ may influence the classification of individual events, the relative variations in sequence summary statistics are insensitive to $\boldsymbol{\eta_0}$ (Zaliapin and Ben-Zion, 2013a). We focus on a subset of 341 crustal earthquake sequences that have mainshock (i.e., largest event) with $M \geq 4.5$ (Figure 1a), which ensures a bandwidth of at least 2 magnitude units between the largest event and the completeness magnitude of 2.5. These sequences only include mainshocks occurring at least six months before the end of our catalog, to prevent artificial truncation of sequences in progress. The separation of the analyzed events into background and clustered earthquakes is shown in Figure 1b.

For each earthquake sequence, we track the faulting style based on the normalized rake angle of the sequence mainshock (Figure 1a). The physical environment in which earthquakes occur is known to influence seismicity and aftershock triggering (e.g., Hauksson, 2011; Hardebeck, 2022). With this in mind, we also compile several geophysical datasets that can be represented as spatial fields that cover our study region (Figure 2). These datasets include: (i) a smoothed representation of surface heat flow in the western US (Mordensky and DeAngelo, 2023), (ii) estimates of subsurface temperature at the median hypocentral depth of each sequence, derived following the method of Shinevar *et al.* (2018), (iii) the second invariant of the strain rate tensor inverted from GNSS data (Kreemer *et al.*, 2014), (iv) depth-to-basement maps, which provide estimates of sedimentary basement thickness (Shah and Boyd, 2018), and (v) the US Geological Survey Quaternary Fault database (see Data and Resources), from which we calculate two surface trace fault complexity metrics (Chu *et al.*, 2021): fault misalignment, a normalized measure of the variability of fault orientations within a geographic region, and fault density, a normalized measure of spatial density of mapped faults within a geographic region. Most of these datasets are motivated primarily by earlier studies of aftershock productivity in southern California (e.g., Yang and Ben-Zion, 2009; Hardebeck, 2022). The fault complexity metrics are new in this context and motivated by the fact that the background stress field and stress changes produced by earthquakes, affecting triggering potential, may depend on both the density and variability in orientation of nearby faults. Recent laboratory experiments, for example, have demonstrated that fault roughness promotes aftershock productivity (Goebel *et al.*, 2023).

Results

To characterize variations in earthquake sequence productivity across California and Nevada, we first count the total number of events in each sequence above the completeness magnitude of 2.5. We then correct for the fact that the total count increases with magnitude ~ 10^{M} (Figure 3a), and define the "sequence productivity factor". This measures, on a log scale, how productive an earthquake sequence is compared to a typical sequence with the same mainshock magnitude. Sequence productivity factors of ~ 0 indicate typical productivity, while factors of +/-1 indicate 10 times more or fewer events produced than expected for a given mainshock magnitude. This is similar to the productivity measure of Dascher-Cousineau et al. (2020), except that it encompasses all events in the sequence rather than just the early aftershocks, to be inclusive of earthquake swarm activity without dominant mainshocks. To improve the robustness and generality of our results, we also consider two alternative productivity metrics: the rate of aftershocks in the first 10 days following the sequence mainshock, and estimates of Omori productivity parameter obtained using the technique of Yang and Ben-Zion (2009). These alternative metrics more directly measure the seismicity rates in the early part of aftershock sequence and productivity of classical aftershock sequences, which have been the focus of previous studies. Since all three metrics are well-correlated (Figure S4), we focus here primarily on the sequence productivity factor.

We observe systematic spatial variations in sequence productivity across California and Nevada (Figure 3b; see Figure S5 for comparable results using the $\mathbf{M} \geq 3$ event subset). As noted by Hardebeck et al. (2018), offshore earthquakes near the Mendocino Triple Junction exhibit unusually low productivity, while events in areas of hydrothermal activity like Coso and the Salton trough exhibit unusually high productivity. Our analysis, which includes several recent prominent earthquake sequences in eastern California and Nevada (e.g., 2019 Ridgecrest, 2020 Monte Cristo, 2021 Antelope Valley), newly highlights the enhanced earthquake productivity of the Walker Lane, the tectonic province that strikes along the California-Nevada border (e.g., Wesnousky, 2005). Previous studies noted the discrepancy between aftershock productivity of northern and southern California (e.g., Reasenberg and Jones, 1989). Including Nevada within a unified analysis framework underscores the difference between the comparatively unproductive sequences along the plate boundary faults in western California and the incipient structures of eastern California and western Nevada. The most productive sequence in our dataset is the 2014-2018 Sheldon earthquake sequence in northwest Nevada (Trugman *et al.*, 2023), which was approximately 100x more productive than a typical sequence with mainshock magnitude 4.8 (Figure 3a).

The spatial pattern of sequence productivity bears some visual relations with the compiled geophysical parameters, particularly heat flow and the two fault complexity metrics: misalignment and density. We can quantify this more formally by computing the statistical correlations between sequence productivity factor and our set of geophysical parameters, spatially interpolated at the sequence locations. For this, we use the Spearman rank correlation coefficient to measure the strength of the relation without assuming a linear correspondence. This analysis (Figure 4) supports the qualitative comparisons in map view: heat flow, fault misalignment, and fault density are all positively correlated with sequence productivity. Temperature and mechanism type show weak negative correlations with productivity, while the correlation of productivity with strain rate and depth-to-basement are negligible.

An important question for hazard assessment is whether there is a relation between sequence productivity and the background rate of earthquake activity. We address this question with our dataset by estimating the background seismicity rate on a spatial grid using the mainshock events identified by the nearest-neighbor method. We find a weak positive correlation between background rate and sequence productivity (Figure S6), but this relation can only account for a small fraction of the observed variance in productivity. Indeed, some locations with the highest rates of background seismicity, like Mendocino and near Los Angeles, have anomalously low productivity.

Discussion

Our analysis newly reveals spatially coherent variations in earthquake sequence productivity across California and Nevada that are correlated with several geophysical parameters, notably surface heat flow, temperature at seismogenic depth, and fault complexity. It is important to recognize that these correlations do not necessarily imply causation; it is possible that there are other factors not considered in this study that control productivity, some of which may correlate with the more readily measurable parameters we examine. Mechanical models can be used to suggest causal relations between properties of the crust and seismicity (e.g., Ben-Zion and Lyakhovsky, 2006), but a definitive demonstration of causality is in general a difficult task.

Nevertheless, we can gain additional insight by developing a statistical model in which different geophysical parameters of interest are used in combination as feature variables to predict sequence productivity as a target variable. Because we do not anticipate these relations to be linear, we use the explicit machine learning algorithm XGBoost (Chen and Guestrin, 2016), which is adept at capturing nonlinear relations but uses a simple enough, tree-based computational framework that permits full model interpretability and is insensitive to the normalization of the input features. To prevent overfitting, we tune model hyperparameters using a Bayesian optimization approach applied to a cross-validation score (Rouet-Leduc *et al.*, 2019). In this approach, the dataset is repeatedly divided into training and testing folds, and the mean-squared error is assessed on data from the testing folds, which the trained model has not seen. The final XGBoost model used in our analysis is trained with the hyperparameters identified from the top-performing models in the cross-validation step.

The performance of the XGBoost model (Figure 5a) is significantly better than is possible through multivariate linear regression applied to the same (normalized) feature variables (Figure S7), with the XGBoost model achieving an R^2 value (i.e., the fraction of data variance explained) of 0.70 compared to 0.29 for multivariate regression. While the XGBoost model predictions are not perfect and tend to be slightly conservative – e.g., underpredicting the productivity of extreme sequences like Sheldon – the model appears to capture sufficiently the statistical relations that we can confidently assess feature importance: i.e., input variables most useful in predicting sequence productivity.

We use for this purpose the SHAP technique (Lundberg and Lee, 2017), which applies a game-theoretical framework to attribute importance scores to the input features of explicit machine learning models like XGBoost. The advantage of SHAP over analogous techniques is its capacity to consistently disentangle effects of multiple input variables that may be mutually correlated.

The attribution scores provided by SHAP are additive, meaning that the sum of the SHAP values for any set of inputs is equal to the target prediction. Averaged across the dataset, larger SHAP values indicate variables that are more important to the model's prediction. For our target variable of sequence productivity that is centered at zero, positive or negative SHAP values imply that the feature value is associated with higher or lower than average productivity, respectively.

The results of this analysis are presented graphically in Figure 5b, where input features are ranked by importance, with the distribution of SHAP values displayed as color-coded points that denote the corresponding feature value. Heat flow is the most important predictive variable, with the clear gradient from blue to red indicating a consistent positive relation with productivity. Temperature, closely followed by fault misalignment and fault density, are ranked next in importance. Temperature has a negative correlation with productivity (colder sequences are more productive), while fault misalignment and fault density have a positive correlation with productivity. The relations between productivity and strain rate, mechanism type, and depth to basement are comparatively weak. The distributions of SHAP values for each feature variable are displayed in Figure 5c, where the nonlinearity of these relationships becomes apparent. For example, the values of highest misalignment are most clearly associated with increased productivity. Likewise, while productivity appears to increase monotonically with heat flow, the extreme values on both the low and high exhibit the strongest relations.

Previous studies in California considered the relation between aftershock statistics and surface heat flow, with somewhat conflicting results. Enescu *et al.* (2009) and Yang and Ben-Zion (2009) present evidence that more productive earthquake sequences occur in regions with lower surface heat flow, while Nandan *et al.* (2017) observe a positive correlation between productivity and heat flow. This discrepancy may arise in part due to data availability – the dataset of Nandan *et al.* (2017) is both more recent and more spatially extensive than those considered by Enescu *et al.* (2009) and Yang and Ben-Zion (2009) – but also may be influenced by modeling assumptions. In particular, Yang and Ben-Zion (2009) measure productivity by estimating Omori parameters from stacked aftershock sequences, Enescu *et al.* (2009) estimated the magnitude-dependent productivity parameter derived from Epidemic Type Aftershock Sequence (ETAS) models, and Nandan *et al.* (2017) solve for spatially-varying ETAS coefficients for their entire study region. The swarm-type sequences may be at the core of the problem, since the Omori parameters are not well-defined for swarms and the ETAS model is also not well-suited to model swarms (Zaliapin and Ben-Zion, 2013b).

Our study uses a productivity metric that avoids the need to assume a particular triggering model like Omori or ETAS, and includes several other geophysical parameters of potential interest. We find a positive correlation between productivity and heat flow, in agreement with Nandan et al. (2017), but also demonstrate that the temperature condition in the seismogenic zone, which depends both on the surface heat flow and the depth of the triggered events, is negatively correlated with productivity. This observation is compatible with the damage rheology model of Ben-Zion and Lyakhovsky (2006) and the results of Yang and Ben-Zion (2009) in which the effective viscosity of the crust controls aftershock statistics. Moreover, we newly identify the importance of faulting complexity with productivity, with more productive earthquake sequences tending to occur in areas with complex and dense networks of mapped Quaternary faults.

It is important to recognize that all the geophysical datasets we consider have spatial limitations, areas of incompleteness, and various forms of uncertainty. For example, heat flow maps are spatially smoothed and may not precisely represent the heat flow observed at any geographic point, while the faulting and strain measurements are derived (primarily) from onshore observations with finite spatial resolution and variable completeness. The Quaternary fault database, while exceptionally detailed in California and Nevada, tracks only surficial features and not the geometry at hypocentral depth. The true strength of the statistical connections between these parameters and productivity are likely to be muted by these limitations, and other parameters not considered in this work, like fluids and local geology, may provide additional insight and could be studied in detail in future work.

We demonstrate that earthquake sequences in the Walker Lane, an incipient zone of deformation along the California-Nevada, are significantly more productive compared to their counterparts along the San Andreas fault system that comprises the present Pacific-North American plate boundary. Across the Walker Lane, earthquake swarms with high seismicity rates are particularly common, where productivity is perhaps further enhanced by the presence of structurally complex and dense networks of active faults. In addition to the geophysical parameters considered in our analysis, this difference may also reflect the anomalously low resolved shear stress on faults of the San Andreas system implied by the lack of observable frictional heat and other evidence summarized by Ben-Zion (2001). Whether or not the obtained relations on earthquake sequence productivity generalize beyond California and Nevada to other crustal faults will need to be assessed in future work. But even within the context of the western United States, the results have important implications for our physical understanding of earthquake triggering and seismic hazard. Developing improved physical or statistical models that accurately capture such systematic regional variations in productivity is an important frontier in earthquake dynamics.

Data and Resources

Earthquake catalog data for this study were obtained from the Southern California Earthquake Data Center (https://service.scedc.caltech.edu/eq-catalogs/date_mag_loc.php), Northern California Earthquake Data Center (https://www.ncedc.org/ncedc/catalog-search.html), and the Nevada Seismological Laboratory (http://www.seismo.unr.edu/Earthquake). The compiled earthquake catalog spanning these monitoring jurisdictions is available on Zenodo (https://doi.org/10.5281/zenodo.8411208). Data processing was performed in Python and Julia, with geographic figures produced using PyGMT (https://www.pygmt.org/dev/overview.html). Quaternary faults and fold data were obtained from the USGS database (https://www.sciencebase.gov/catalog/item/589097b1e4b072a7ac0cae23).

Acknowledgments

This work would not have been possible without the pioneering work of our dear friend and colleague Ilya Zaliapin. This paper is dedicated to Ilya's memory. We thank T. Goebel, an anonymous reviewer, and the Associate Editor for constructive comments that improved the manuscript. This work also benefited from scientific conversations with S. Wesnousky, B. Savran, K. Smith, G. Hirth, V. Tsai, A. Chatterjee, J. Lee, C. Marone, V. Lambert, and W. Marzocchi. The study was supported by the National Science Foundation (awards EAR-2231705, EAR-2121666, and EAR-2122168) and the Nevada Division of Emergency Management award HMGP DR-4523-08-08P.

References

Ben-Zion, Y. (2008). Collective behavior of earthquakes and faults: Continuum-discrete transitions, progressive evolutionary changes, and different dynamic regimes, *Reviews of Geophysics* **46**, no. 4, doi: 10.1029/2008RG000260.

Ben-Zion, Y. (2001). Dynamic ruptures in recent models of earthquake faults, *Journal of the Mechanics and Physics of Solids* **49**, no. 9, 2209–2244, doi: 10.1016/S0022-5096(01)00036-9.

Ben-Zion, Y., and V. Lyakhovsky (2006). Analysis of aftershocks in a lithospheric model with seismogenic zone governed by damage rheology, *Geophysical Journal International* **165**, no. 1, 197–210, doi: 10.1111/j.1365-246X.2006.02878.x.

Chen, T., and C. Guestrin (2016). XGBoost: A Scalable Tree Boosting System, *Proceedings of the 22nd ACM SIGKDD International Conference on Knowledge Discovery and Data Mining*, 785–794, doi: 10.1145/2939672.2939785.

Chu, S. X., V. C. Tsai, D. T. Trugman, and G. Hirth (2021). Fault interactions enhance high-frequency earthquake radiation, *Geophysical Research Letters* **46**, e2021GL095271, doi: 10.1029/2021GL095271.

Dascher-Cousineau, K., E. E. Brodsky, T. Lay, and T. H. W. Goebel (2020). What Controls Variations in Aftershock Productivity?, *Journal of Geophysical Research: Solid Earth* **125**, no. 2, e2019JB018111, doi: 10.1029/2019JB018111.

Davis, S. D., and C. Frohlich (1991). Single-link cluster analysis of earthquake aftershocks: Decay laws and regional variations, *Journal of Geophysical Research: Solid Earth* **96**, no. B4, 6335–6350, doi: 10.1029/90JB02634.

Enescu, B., S. Hainzl, and Y. Ben-Zion (2009). Correlations of Seismicity Patterns in Southern California with Surface Heat Flow Data, *Bulletin of the Seismological Society of America* **99**, no. 6, 3114–3123, doi: 10.1785/0120080038.

Goebel, T. H. W., E. E. Brodsky, and G. Dresen (2023). Fault Roughness Promotes Earthquake-Like Aftershock Clustering in the Lab, *Geophysical Research Letters* **50**, no. 8, e2022GL101241, doi: 10.1029/2022GL101241.

Goebel, T. H. W., Z. Rosson, E. E. Brodsky, and J. I. Walter (2019). Aftershock deficiency of induced earthquake sequences during rapid mitigation efforts in Oklahoma, *Earth and Planetary Science Letters* **522**, 135–143, doi: 10.1016/j.epsl.2019.06.036.

Hardebeck, J. L. (2022). Physical Properties of the Crust Influence Aftershock Locations, *Journal of Geophysical Research: Solid Earth* **127**, no. 10, e2022JB024727, doi: 10.1029/2022JB024727.

Hardebeck, J. L., A. L. Llenos, A. J. Michael, M. T. Page, and N. van der Elst (2018). Updated California Aftershock Parameters, *Seismological Research Letters* **90**, no. 1, 262–270, doi: 10.1785/0220180240.

Hauksson, E. (2011). Crustal geophysics and seismicity in southern California, *Geophysical Journal International* **186**, no. 1, 82–98, doi: 10.1111/j.1365-246X.2011.05042.x.

Hill, D. P. (1977). A model for earthquake swarms, *Journal of Geophysical Research (1896-1977)* **82**, no. 8, 1347–1352, doi: 10.1029/JB082i008p01347.

Kreemer, C., G. Blewitt, and E. C. Klein (2014). A geodetic plate motion and Global Strain Rate Model, *Geochemistry, Geophysics, Geosystems* **15**, no. 10, 3849–3889, doi: 10.1002/2014GC005407.

Lundberg, S. M., and S.-I. Lee (2017). A unified approach to interpreting model predictions, in *Advances in neural information processing systems* I. Guyon, U. V. Luxburg, S. Bengio, H. Wallach, R. Fergus, S. Vishwanathan, and R. Garnett(Editors), Curran Associates, Inc., 4765–4774.

Mordensky, S. P., and J. DeAngelo (2023). Geothermal resource favorability: select features and predictions for the western United States curated for DOI 10.1016/j.geothermics.2023.102662, U.S. Geological Survey, doi: 10.5066/P9V1Q9XM.

Nandan, S., G. Ouillon, S. Wiemer, and D. Sornette (2017). Objective estimation of spatially variable parameters of epidemic type aftershock sequence model: Application to California, *Journal of Geophysical Research: Solid Earth* **122**, no. 7, 5118–5143, doi: 10.1002/2016JB013266.

Omori, F. (1894). Investigation of aftershocks, *Rep. Earthquake Inv. Comm* **2**, 103–139.

Page, M. T., N. van der Elst, J. Hardebeck, K. Felzer, and A. J. Michael (2016). Three Ingredients for Improved Global Aftershock Forecasts: Tectonic Region, Time-Dependent Catalog Incompleteness, and Intersequence Variability, *Bulletin of the Seismological Society of America* **106**, no. 5, 2290–2301, doi: 10.1785/0120160073.

Reasenberg, P. A., and L. M. Jones (1989). Earthquake Hazard After a Mainshock in California, *Science* **243**, no. 4895, 1173–1176, doi: 10.1126/science.243.4895.1173.

Rouet-Leduc, B., C. Hulbert, and P. A. Johnson (2019). Continuous chatter of the Cascadia subduction zone revealed by machine learning, *Nature Geoscience* **12**, no. 1, 75, doi: 10.1038/s41561-018-0274-6.

Shah, A. K., and O. S. Boyd (2018). Depth to basement and thickness of unconsolidated sediments for the western United States - Initial estimates for layers of the U.S. Geological Survey National Crustal Model, Open-File Report 1115, U.S. Geological Survey, doi: 10.3133/ofr20181115.

Shinevar, W. J., M. D. Behn, G. Hirth, and O. Jagoutz (2018). Inferring crustal viscosity from seismic velocity: Application to the lower crust of Southern California, *Earth and Planetary Science Letters* **494**, 83–91, doi: 10.1016/j.epsl.2018.04.055.

Singh, S. K., and G. Suárez (1988). Regional variation in the number of aftershocks (mb $\geqq$ 5) of large, subduction-zone earthquakes (Mw $\geqq$ 7.0), *Bulletin of the Seismological Society of America* **78**, no. 1, 230–242, doi: 10.1785/BSSA0780010230.

Trugman, D., W. Savran, C. Ruhl, and K. Smith (2023). Unraveling the Evolution of an Unusually Active Earthquake Sequence Near Sheldon, Nevada, 2, *Seismica* **2**, no. 2, doi: 10.26443/seismica.v2i2.1051.

Wesnousky, S. G. (2005). Active faulting in the Walker Lane, *Tectonics* **24**, no. 3, doi: 10.1029/2004TC001645.

Yang, W., and Y. Ben-Zion (2009). Observational analysis of correlations between aftershock productivities and regional conditions in the context of a damage rheology model, *Geophysical Journal International* **177**, no. 2, 481–490, doi: 10.1111/j.1365-246X.2009.04145.x.

Zaliapin, I., and Y. Ben-Zion (2016). A global classification and characterization of earthquake clusters, *Geophysical Journal International* **207**, no. 1, 608–634, doi: 10.1093/gji/ggw300.

Zaliapin, I., and Y. Ben-Zion (2013a). Earthquake clusters in southern California I: Identification and stability, *Journal of Geophysical Research: Solid Earth* **118**, no. 6, 2847–2864, doi: 10.1002/jgrb.50179.

Zaliapin, I., and Y. Ben-Zion (2013b). Earthquake clusters in southern California II: Classification and relation to physical properties of the crust, *Journal of Geophysical Research: Solid Earth* **118**, no. 6, 2865–2877, doi: 10.1002/jgrb.50178.

Zaliapin, I., A. Gabrielov, V. Keilis-Borok, and H. Wong (2008). Clustering Analysis of Seismicity and Aftershock Identification, *Phys. Rev. Lett.* **101**, no. 1, 018501, doi: 10.1103/PhysRevLett.101.018501.

Mailing Addresses:

<u>Daniel T. Trugman</u>: Nevada Seismological Laboratory, University of Nevada, Reno. 1664 N Virginia St., Reno NV 89557.

Yehuda Ben-Zion: Department of Earth Science and Statewide California Earthquake Center, University of Southern California. 3651 Trousdale Parkway #169 Los Angeles, CA 90089-0742.

Figures

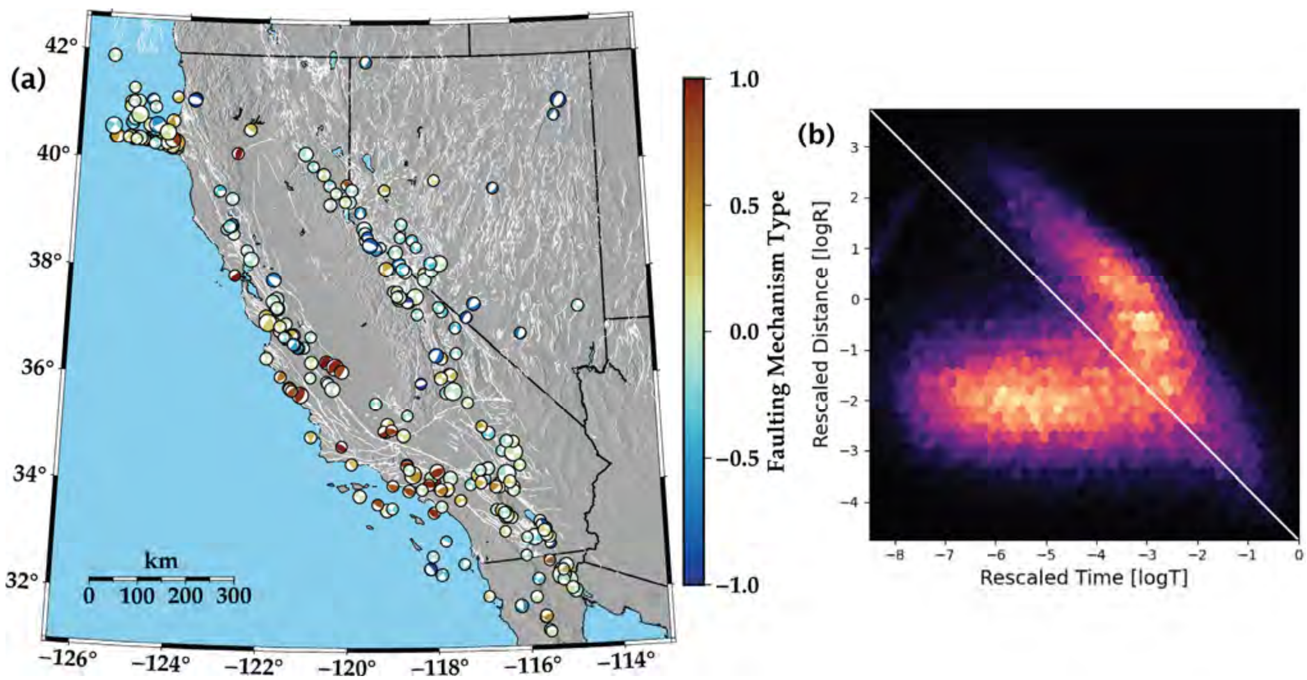

Figure 1. (a) Overview map of the study region with **M** ≥ 4.5 sequences analyzed in this study denoted by their mainshock mechanism and color-coded by mechanism type, where values of -1, 0 and 1 correspond to normal, strike-slip, and reverse faulting, respectively. (b) Graphical representation of the distribution of nearest-neighbor rescaled distance $10^{-0.5bM_i}\,R_{ij}$ versus rescaled time $10^{-0.5bM_i}\,T_{ij}$, plotted on a log-log with the cutoff threshold used in this study marked as a solid line.

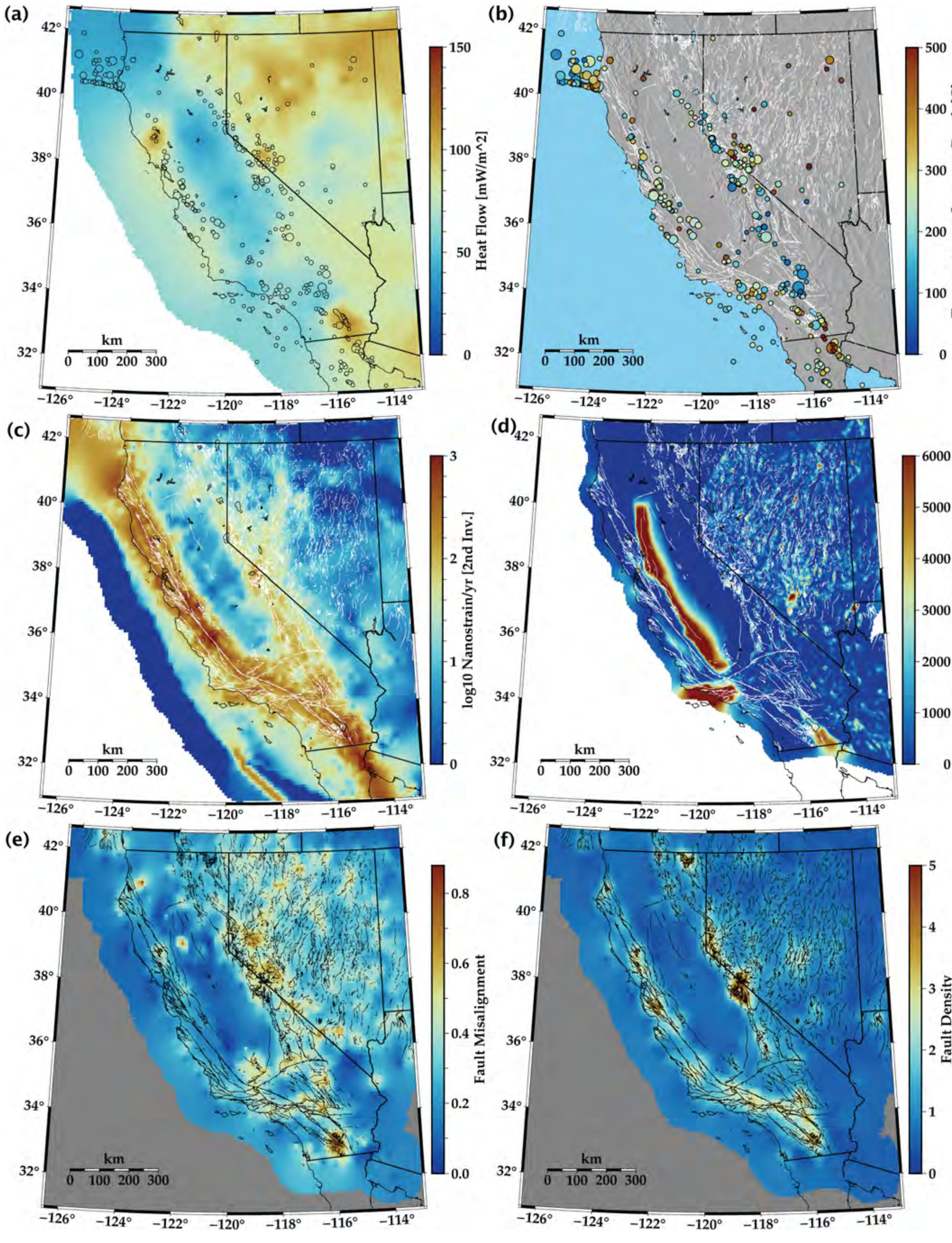

(a)
Heat Flow [mW/m^2]
(b)
Temperature at Sequence Depth [C]
(c)
log10 Nanostrain/yr [2nd Inv.]
(d)
Depth to Basement [m]
(e)
Fault Misalignment
(f)
Fault Density
km
0 100 200 300

Figure 2. Map view representations of geophysical parameters in the western US: (a) surface heat flow, (b) temperature at the seismogenic depth of each sequence, (c) second invariant of the strain rate tensor, (d) depth to crystalline basement, (e) fault misalignment, (f) fault density.

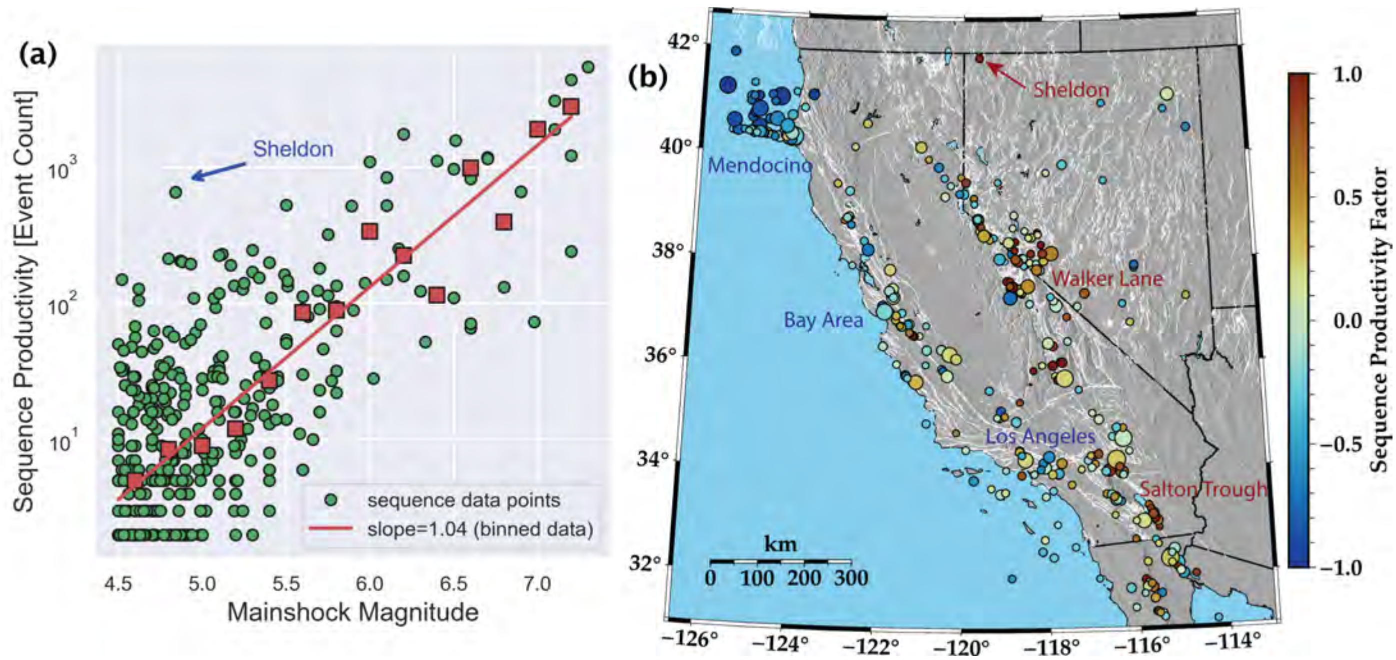

Figure 3. (a) Scaling of total sequence productivity with magnitude, with individual sequences marked in green and binned data marked in red. The sequence productivity factor metric used in this study corrects for this trend and measures the deviation from expected productivity at a given mainshock magnitude (red line), on a logarithmic scale. (b) Map view representations of sequence productivity factors. Productivity is higher in eastern California and the Walker Lane than in western California and offshore Mendocino.

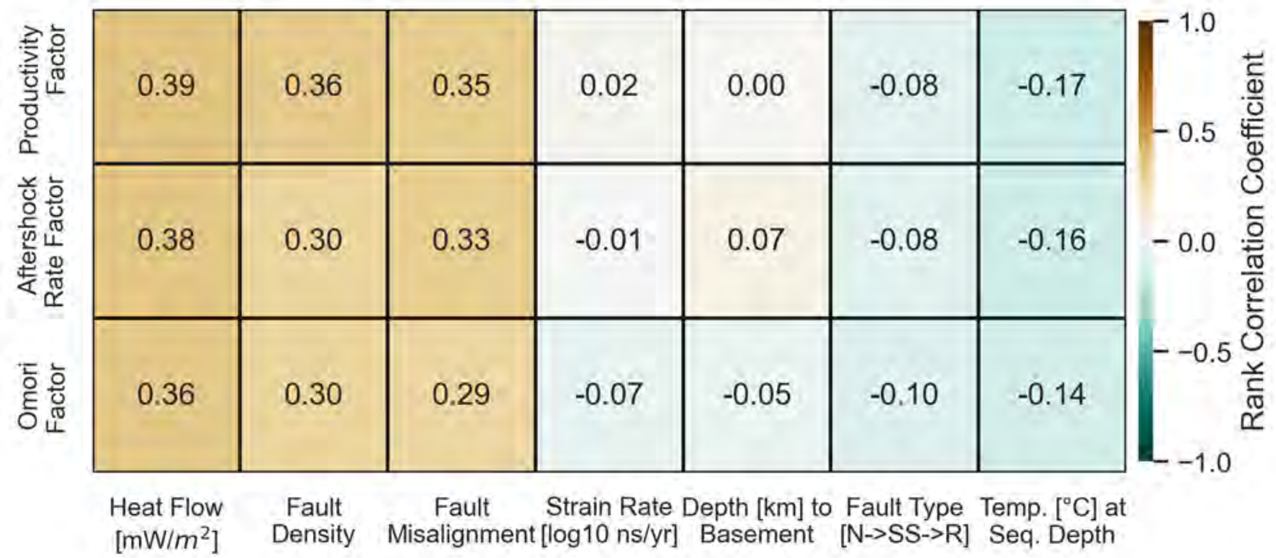

Figure 4. Correlation matrix between geophysical parameters (columns) and sequence productivity factor (top row) as well as alternative productivity metrics: aftershock rate and Omori parameter (middle and bottom rows). Warm and cool colors indicate positive and negative rank correlations, respectively.

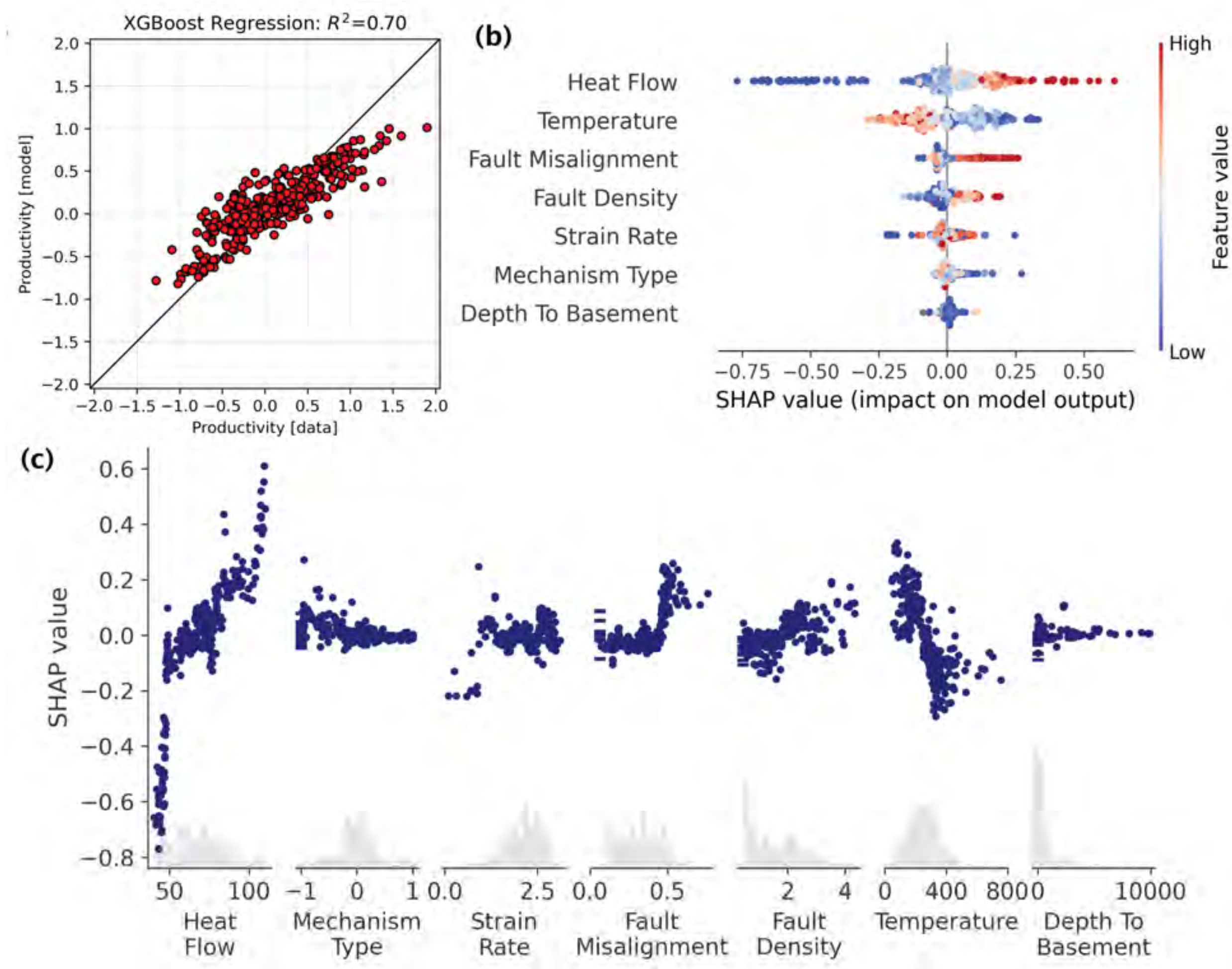

Figure 5. Machine learning analysis of earthquake sequence productivity. (a) Performance of the XGBoost model for predicting sequence productivity, plotting measured productivity factors on the x-axis versus model predictions on the y-axis. (b) SHAP value distributions (x-axis) for each input feature, ranked by importance and with individual observations color-coded by relative feature values (low to high). The spread of the SHAP value distribution along the x-axis indicates the magnitude of the feature importance, while the colorscale can be used to identify the sign of the relation between feature value and SHAP value. (c) SHAP values plotted as a function of each geophysical input feature, highlighting nonlinear relations discernable in (b). Feature values associated with negative and positive SHAP values are associated with lower or higher predicted values of sequence productivity, respectively.

Electronic Supplement to:

Coherent Spatial Variations in the Productivity of Earthquake Sequences in California and Nevada

By Daniel T. Trugman and Yehuda Ben-Zion

Overview

This document contains supplementary figures that support the results presented in the main text.

Figure S1 shows the data used to infer magnitude of completeness for the combined catalogs. Figure S2 displays other catalog statistics, including moment/network magnitude relations, estimates of b-value and fractal dimension to support the parameters used in this study. Figure S3 shows the nearest-neighbor distance distribution used to determine an appropriate threshold to separate clustered from background seismicity. Figure S4 compares different measures of productivity. Figure S5 presents results for an M3+ event subset of the M2.5+ dataset focused on in the main text. Figure S6 displays the relation between background rate and sequence productivity. Figure S7 compares multivariate linear regression and XGBoost models to predict sequence productivity.

Figures

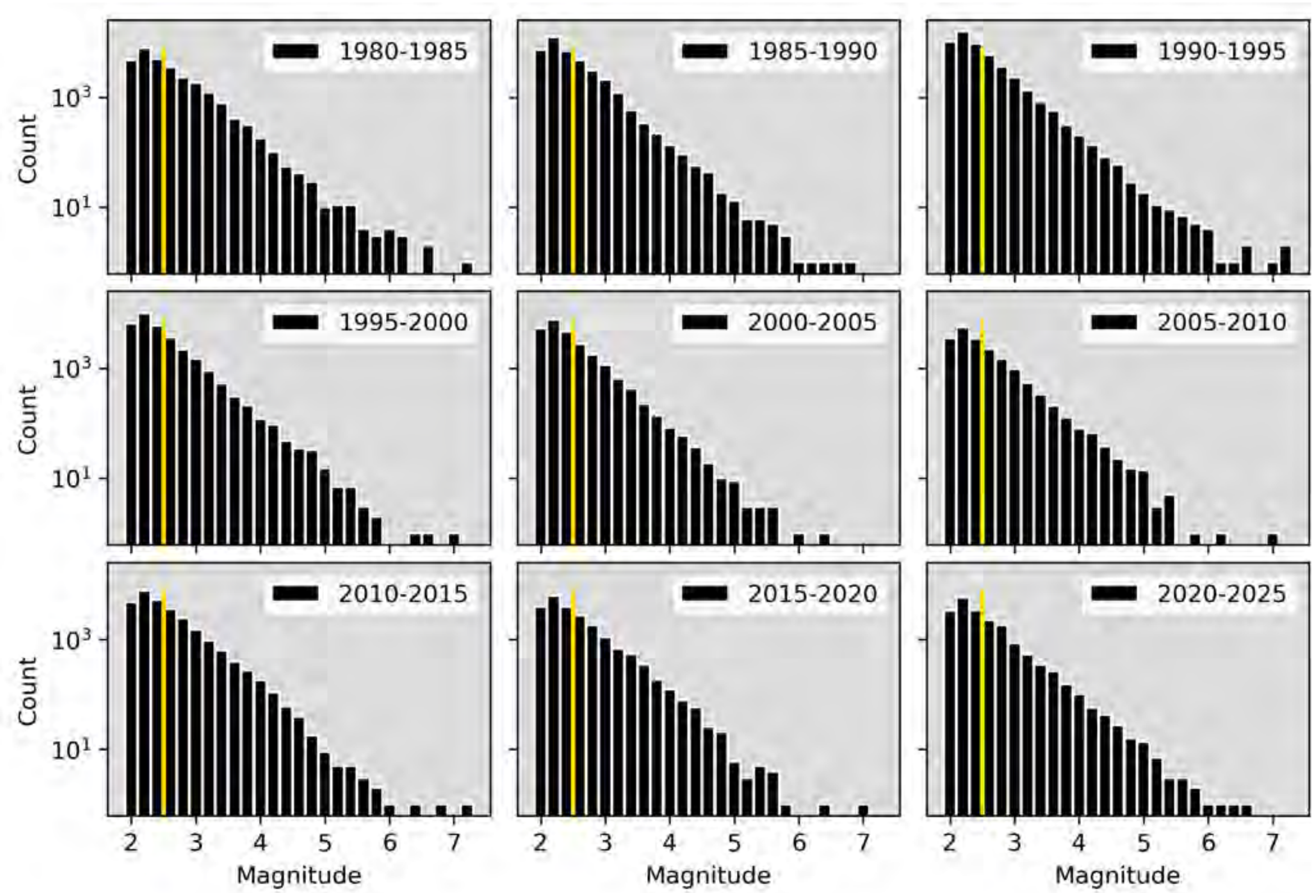

Figure S1. Magnitude distributions of the combined California-Nevada earthquake catalog within different time periods. Estimates for the magnitude of completeness of each time period, obtained from the maximum curvature approach with a shift of 0.3 units, are marked in gold and is **M**2.5 or less for all time periods.

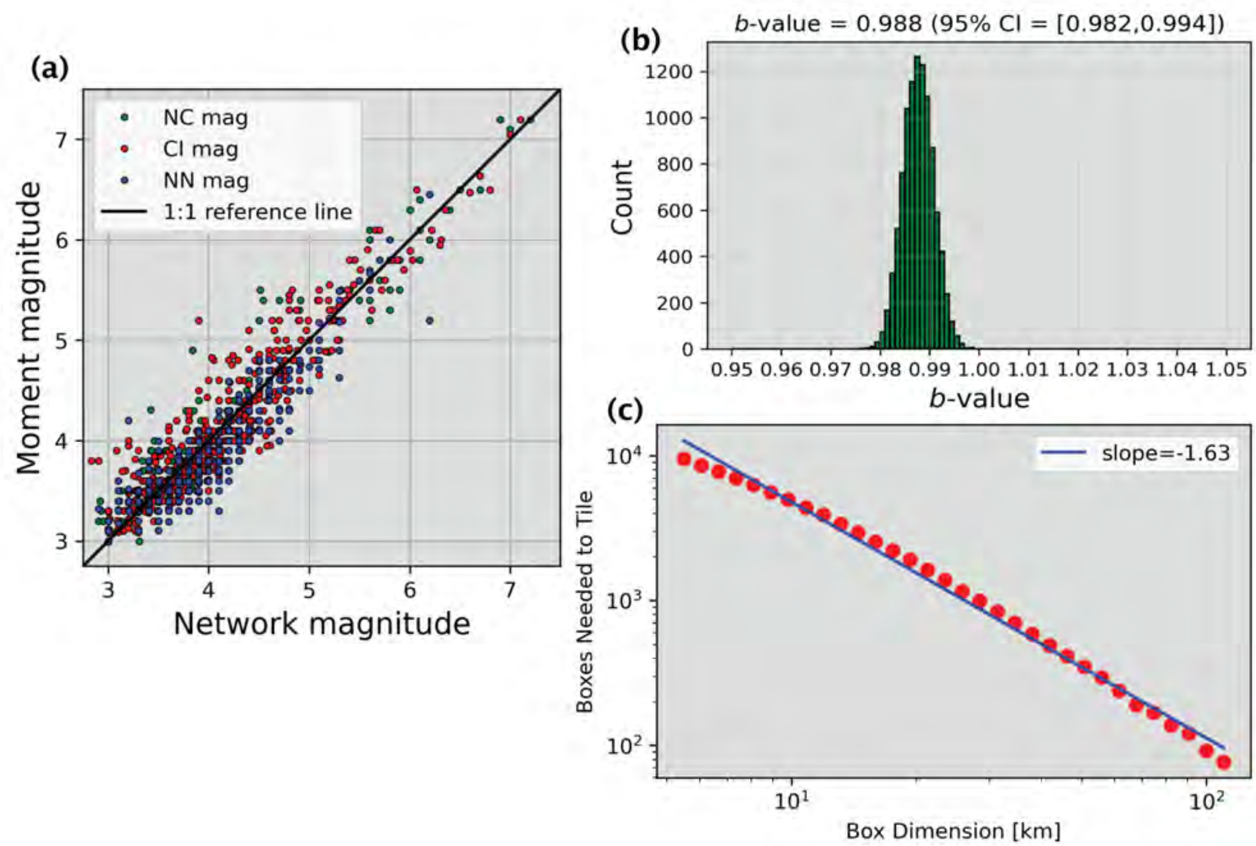

Figure S2. (a) Relation between magnitude estimate by individual seismic networks (NC=Northern California, CI=Southern California, NN=Nevada) and moment magnitude. For **M**3 and greater, the network magnitudes are consistent with M_W and fall along the 1:1 line. (b) Estimation of (b) b-value using the maximum-likelihood method and bootstrap resampling to obtain uncertainties, and (c) fractal dimension estimation using a standard box-counting approach. These results support the parameter values used in the nearest neighbor analysis in this study.

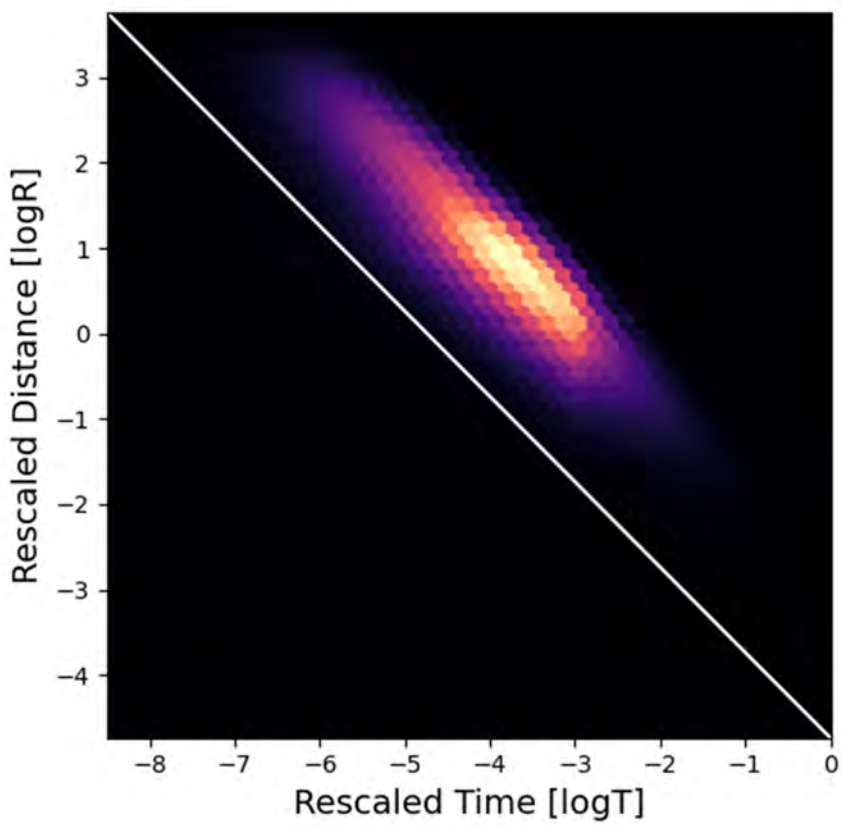

Figure S3. Distribution of rescaled nearest neighbor distances from 100 stacked space-time shuffled versions of the combined California-Nevada catalog analyzed in this study. In each shuffled dataset, magnitudes are preserved. The selected threshold distance of -4.75 (in log unit) comes from the 2nd percentile of the nearest-neighbor distribution of the stacked catalogs.

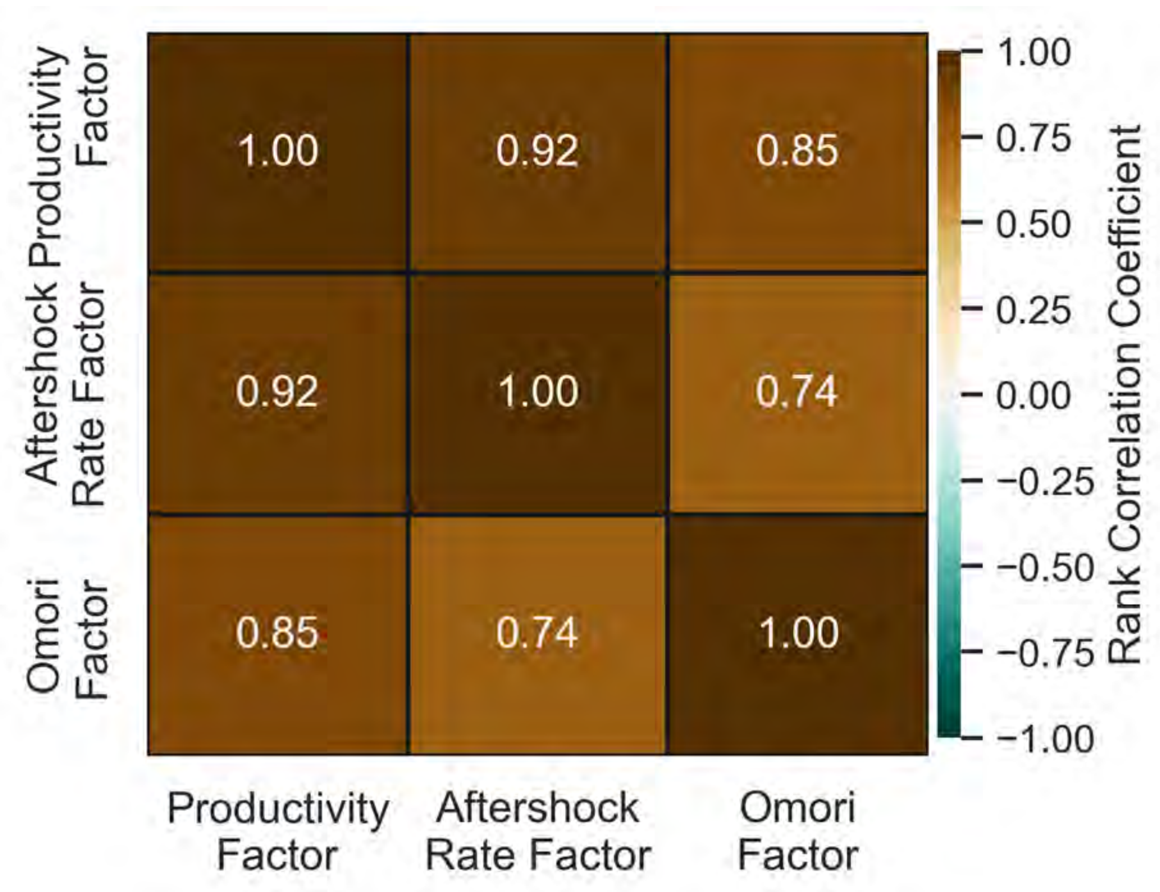

Figure S4. Correlation matrix between three different measures of productivity: sequence productivity factor, aftershock rate, and Omori parameter. The sequence productivity factor is the primary focus of this study and correlates with aftershock rate and Omori parameter at the 0.92 and 0.85 level.

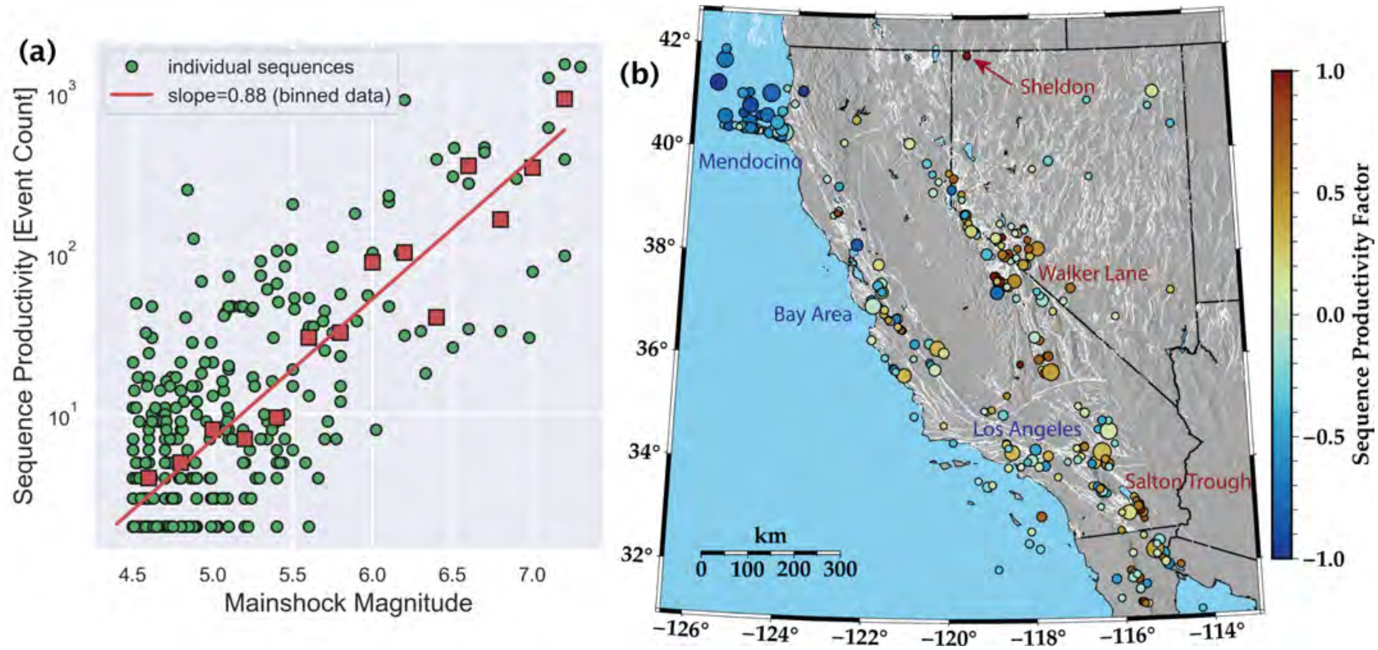

Figure S5. Sequence productivity measures for **M**3+ seismicity, analogous to Figure 3 in the main text which uses **M**2.5+ seismicity. The similarity of the spatial patterns implies that the overall findings are robust to the choice of minimum magnitude.

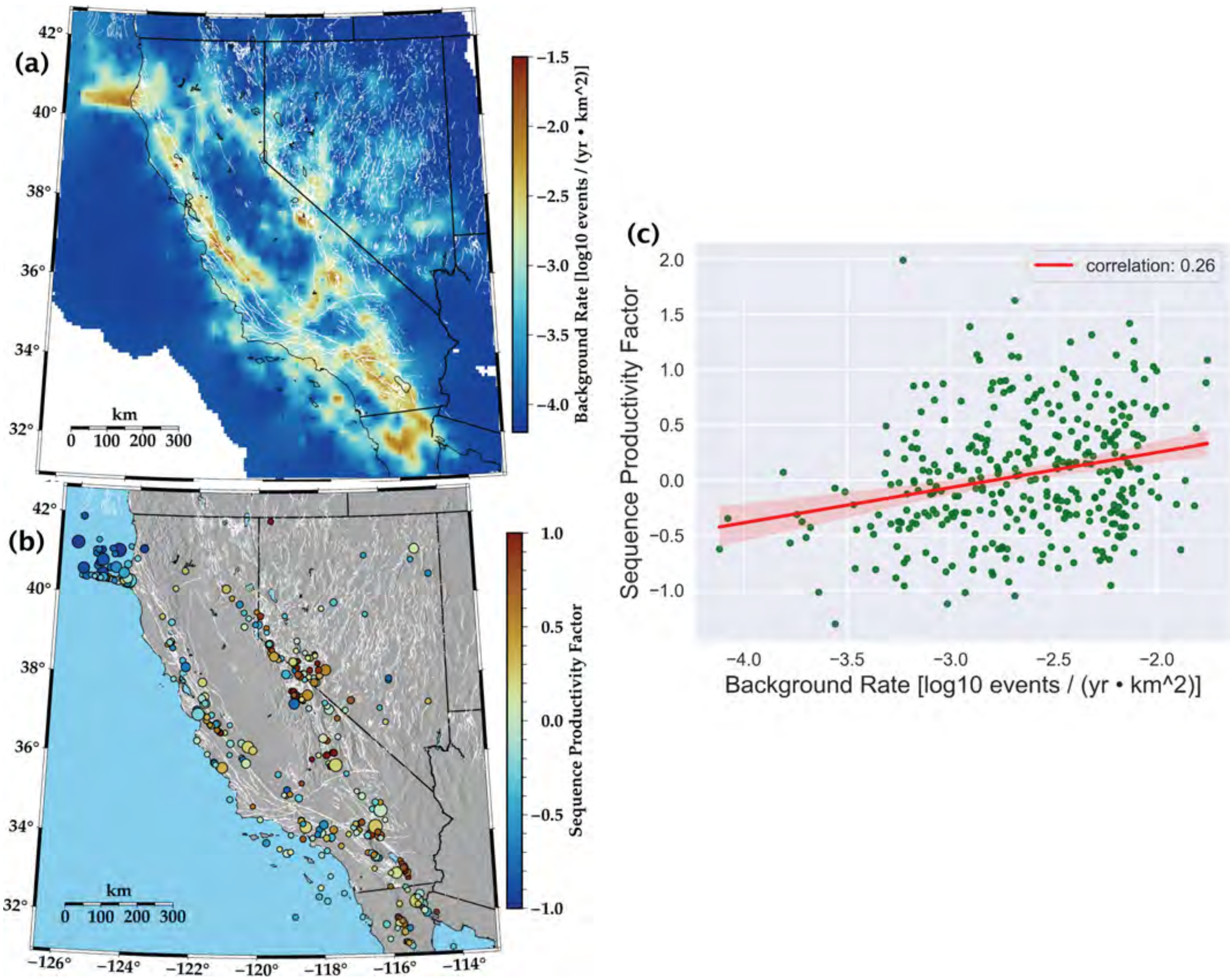

Figure S6. Comparison of (a) background seismicity rate, inferred from the spatial pattern of mainshocks identified by the nearest-neighbor analysis with (b) sequence productivity factors, as displayed in Figure 3 of the main text. There is a weak positive correlation (c), but much of the scatter in productivity is not explained by variations in background rate.

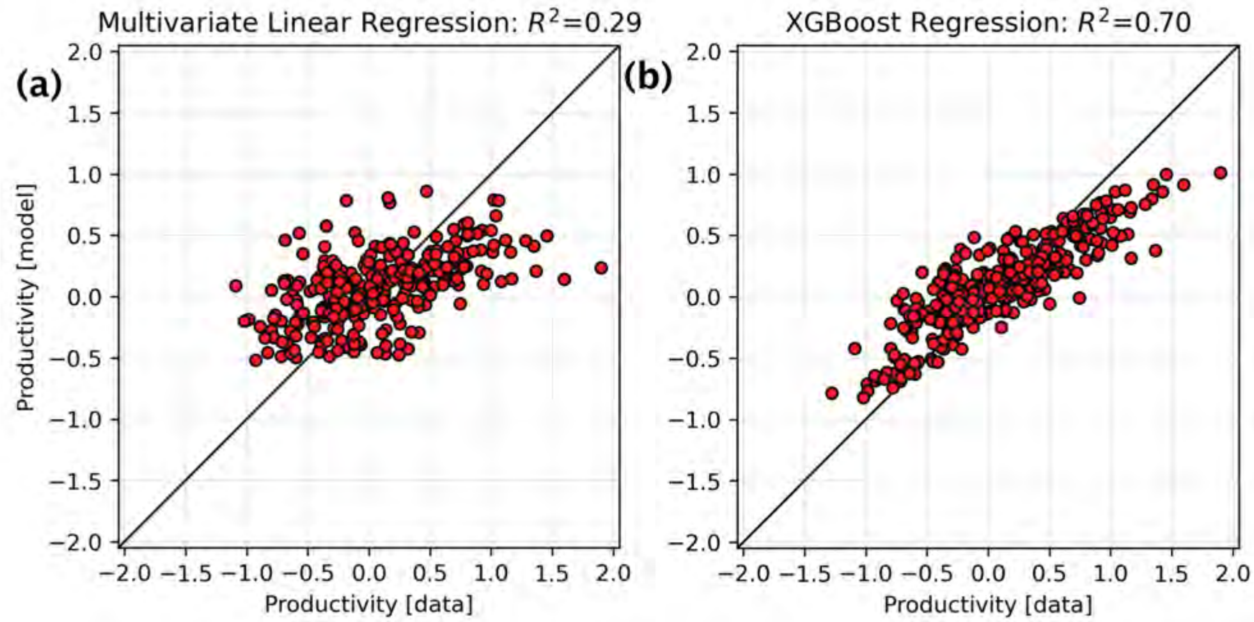

Figure S7. Comparison of model performance of (a) multivariate linear regression and (b) XGBoost regression, with hyperparameters optimized through a Bayesian cross-validation scheme. The XGBoost model vastly outperforms the multivariate linear model and does not require normalization of the input features. The R^2 statistic (related to the fraction of variance explained) is listed in each figure panel title: 0.29 for multivariate linear regression and 0.70 for XGBoost.